Proceedings of ASME Turbo Expo 2011
GT2011
June 6-10, 2011, Vancouver, British Columbia, Canada

GT2011-46709

EXPERIMENTAL SIMULATION OF CONTAMINANT DEPOSITION ON A FILM COOLED TURBINE VANE PRESSURE SIDE WITH A TRENCH

Jason E. Albert and David G. Bogard
University of Texas at Austin
Austin, Texas, USA

ABSTRACT

An important issue in the use of coal- or biomass-derived synthetic gaseous (syngas) fuels is the deposition of contaminants on film cooled turbine surfaces, which alter cooling and aerodynamic performance and increase material degradation. The current study applied a new experimental technique that simulated the key physical aspects of contaminant deposition on a film cooled turbine vane. The depositing contaminants were modeled in a wind tunnel facility with a spray of molten wax droplets of a size range that matched the Stokes number of the contaminant particles in engine conditions. Most experiments were performed using a vane model with a thermal conductivity selected such that the model had the same Biot number of an actual engine airfoil, resulting in a cooler surface temperature. Some experiments were performed using an approximately adiabatic model for comparison. The film cooling design consisted of three rows of showerhead cooling at the leading edge and one row of body film cooling holes on the pressure side. Two designs of pressure side body film cooling holes were considered: a standard design of straight, cylindrical holes and an advanced design of "trenched" cooling holes in which the hole exits were situated in a recessed, transverse trench.

The results showed thin deposits formed in the trench, with the thickest deposits on its downstream wall between coolant jets. Adiabatic film effectiveness levels were essentially unchanged by the presence of deposits for either film configuration. Deposit formation was strongly influenced by the model surface temperature with cooler surfaces inhibiting deposition. There was evidence of a threshold surface temperature above which deposits became significantly thicker.

NOMENCLATURE

Bi	Biot number, $h_g t_{wall}/k_g$
C	airfoil chord length (stagnation point to tail point)
d	cooling hole diameter or particle diameter
DR	coolant-to-mainstream density ratio, ρ_c/ρ_∞
h	convective heat transfer coefficient
H	trench depth
k	thermal conductivity
l	length
M	blowing (mass flux) ratio, $\rho_c U_c/(\rho_\infty U_\infty)_{local}$
M^*	showerhead blowing (mass flux) ratio, $\rho_c U_c/(\rho_\infty U_\infty)_{approach}$
PS	pressure (concave) side of airfoil
Re	Reynolds number
Shd	showerhead
SS	suction (convex) side of airfoil
t	thickness
T	temperature
Tu	turbulence intensity
U	velocity
z	spanwise distance along model surface

Greek:

α	cooling hole surface angle
β	cooling hole compound angle, relative to streamwise
δ	uncertainty
η	adiabatic film effectiveness, $(T_\infty-T_{aw})/(T_\infty-T_c)$
ϕ	overall cooling effectiveness, $(T_\infty-T_{surf})/(T_\infty-T_c)$
Λ	turbulence integral length scale
μ	dynamic viscosity
ρ	density

Subscripts:

aw	adiabatic wall surface
c	coolant
$char$	characteristic length or velocity

dep	deposit
f	with film cooling
g	gas
p	particle
o	without film cooling
solid	solidification
surf	model surface
∞	mainstream

INTRODUCTION

Gas turbine engines for all applications are subject to deposition, erosion, and corrosion (DEC) from contaminants introduced by the inlet air (e.g. sand, salt, debris) and the fuel (e.g. ash particles, impurities). DEC is a particularly important issue for the combustion gas turbine engines in integrated gasification combined cycle (IGCC) power plants due to their use of synthetic gaseous (syngas) fuels derived from raw energy sources such as coal and biomass.

Deposition is typically the dominant mode of DEC degradation for the high pressure turbine airfoils because the higher gas temperatures make the contaminant particles softer and stickier. Deposits on turbine airfoils increase surface roughness and decrease aerodynamic and cooling efficiencies. Deposits also alter film cooling performance, and they can chemically degrade airfoil materials. High pressure turbine airfoils are very reliant on film cooling, due to the higher temperatures they must withstand. Therefore, the interaction between contaminant deposition and film cooling is particularly important for these critical turbine airfoils. The motivation for the current study is to better understand this interaction in order to mitigate the adverse effect of the deposits on cooling efficiency. The application of primary interest in this study is a combustion gas turbine in an IGCC power plant burning coal-derived syngas.

The deposition of ash on coal-fired furnace and gas turbine engine surfaces has been studied by numerous researchers during the past several decades. The theoretical basis to explain and predict coal ash deposit growth has been largely motivated by coal furnace applications, with specific attention given to cylindrical steam-cooled boiler tubes subjected to a cross-flow of contaminant-laden air. Particularly relevant to the current study is the work of Walsh *et al.* [1] that developed an analytical model for estimating deposit growth on a steam-cooled tube of a coal-fired furnace and generated experimental data to test and calibrate the model. Similar to other previous studies, (e.g. Rosner and Nagarajan [2]), Walsh *et al.* noted that coal ash deposition is dependent on the presence of molten and/or sticky particles in the contaminants. Their analytical model includes the warming of the deposit surface temperature caused by the thermal resistance of the underlying deposit thickness, which results in a softer surface that captures more impacting particles. They also account for the reduction in deposit growth rate caused by erosion of the existing deposit by solidified contaminants striking the surface. They note that the mass of deposit per unit area surface can approach an equilibrium value at which deposition is balanced by erosion. Rosner and Nagarajan [2] also recognized this "self-regulating" effect of erosion on deposition.

Wenglarz and Fox [3] performed an experimental study of coal ash deposition in gas turbines specifically considering the use of coal-water fuels. They found a dramatic increase in deposit growth rate when the gas temperature changed from 1260 K to 1370 K. They speculated this increased rate was caused by a higher number of molten or softened particles in the higher temperature flow. Furthermore, they found that increasing the model surface temperature from 1170 K to 1370 K (for a gas temperature of 1370 K) caused a significant increase in deposit growth rate. The data reported by Wenglarz and Fox [3] were in terms in deposit growth rates, and no mention was made of an equilibrium deposit thickness.

A series of experimental studies regarding syngas ash deposition in gas turbines has been performed using the Turbine Accelerated Deposition Facility (TADF) developed by Bons, Fletcher, and colleagues. This facility used engine-representative flow conditions and ash chemistry to generate turbine deposits in an accelerated manner. Crosby *et al.* [4] used the TADF to study how deposits were affected by particle size, gas temperature, and target surface temperature. They found that deposit growth increased with gas temperature above a threshold of about 1230 K. Furthermore, both deposit growth and deposit roughness decreased as the target surface temperature decreased for a given gas temperature. Ai *et al.* [5] performed a study with the TADF exploring the effect of particle size and film cooling flows on deposition. Film cooling arrangements consisted of standard round film holes of varying pitches and blowing ratios, as well as a trench configuration discussed later in this section. The film cooled target surface was a flat coupon oriented at 45° to the impinging hot gas flow. Increased blowing ratio caused decreased deposit growth and decreased roughness. The reduced deposition appeared to be due to a combination of the film cooling jets and to the lower target surface temperature caused by backside cooling flow. At the highest blowing ratio (i.e., coldest surface temperature), the surface had very thin deposits relative to other cases. Lewis *et al.* [6] measured adiabatic film effectiveness and heat transfer augmentation in a wind tunnel facility using three different large-scale models of TADF-generated deposits near standard film cooling holes. One deposit model was similar to a ramp upstream of the cooling holes, and this caused enhanced film cooling performance due to the effects of a separation region near the film hole exits. The other two models had thick or thin deposits upstream and between the film cooling streaks, which resulted in only small changes in film cooling performance. No limiting values of deposit coverage or thickness were reported for any of the TADF studies.

An experimental technique to model contaminant deposition on an airfoil surface was developed recently by Albert *et al.* [7], who first applied it in a turbine blade leading edge experimental facility. The current study utilizes the same technique described in Albert *et al.*, but applied to a different wind tunnel facility modeling the full airfoil of a turbine vane.

This work has been performed in collaboration with Lawson and Thole [8] who developed and applied a similar technique to study deposition on turbine endwall surfaces. Their measurements showed deposits causing a decrease in adiabatic film effectiveness for a range of blowing ratios. The deposit generated by Lawson and Thole showed symptoms of secondary flow structures at the endwall, such as the vortex and saddle point near the airfoil leading edge.

A film cooling design of interest to the current study is "trenched" film cooling, in which a row of straight, cylindrical cooling holes is situated in a transverse, recessed trench with a rectangular cross-section. Bunker [9] first published the concept of trenched film cooling, which included limited data regarding the increase in performance. This data was recorded using a flat plate wind tunnel facility. Trenched film cooling was experimentally studied in greater detail by Waye and Bogard [10], who found a significant enhancement of film cooling effectiveness for a trenched configuration compared to a comparable conventional design without a trench. This enhanced performance was attributed to the film coolant jets impinging on the downstream wall of the trench, spreading laterally within the trench, and forming a fairly continuous layer of film coolant (and high film effectiveness) downstream of the trench. Dorrington *et al.* [11] studied an expanded range of trench geometries, resulting in improved performance compared to that reported by Waye and Bogard. Their data showed that film effectiveness improved with trench depth, with most of the improvement occurring up to a depth of H/d = 0.75. They also showed that performance was fairly insensitive to slight increases in trench depth beyond the length of the cooling hole footprint. The results of Dorrington *et al.* are the basis for selecting the trench geometry used in the current study.

Ai *et al.* [5] used the TADF to generate deposits on a target coupon with film cooling holes situated in a narrow, transverse trench. An important difference with the configuration used in their work was the mainstream flow impacted the test coupon at an angle. The trench configuration tested by Ai *et al.* accumulated significantly more deposit than standard film cooling holes, yet the cooling performance remained about the same. The deposits in the trench primarily grew from the remaining portions of the downstream wall of the trench between the missing notches.

The objective of the current study was to experimentally simulate contaminant deposition on a film cooled turbine vane airfoil leading edge and pressure side in order to assess how the deposit formation was influenced by the presence of film cooling. These simulations were performed for a vane with showerhead and pressure side film cooling, with an emphasis on comparing an advanced trenched cooling hole design to a more conventional design.

EXPERIMENTAL FACILITIES AND PROCEDURES

The experimental facility for the current study was described in some detail by Albert and Bogard [12]. Select portions of that description are included in this paper for completeness.

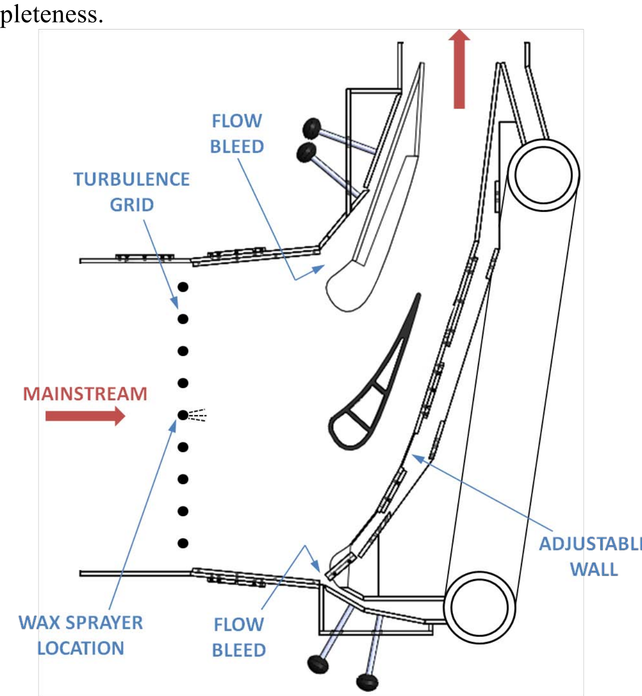

Figure 1. Wind tunnel test section schematic

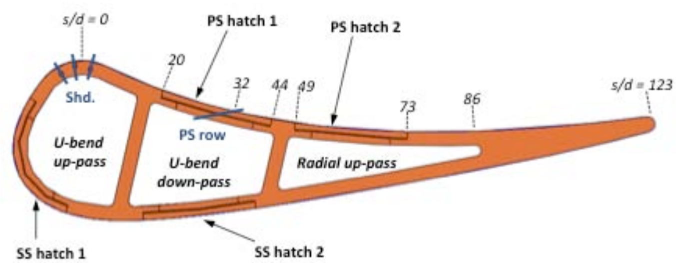

Figure 2. Vane model cross-section schematic with hatch locations shown

All experiments for this study were performed in a closed-loop wind tunnel facility. The wind tunnel mainstream flow was driven by 50 hp variable speed motor and fan, after which the flow passed through an arrangement of desiccant packs, a water-regulated heat exchanger, a series of honeycomb and screen partitions, and an area contraction before entering the test section. The test section incorporated a two-passage vane cascade with the full vane model in the middle being the test airfoil, as shown in Fig. 1. A passive grid turbulence generator was situated at the entrance to the test section. It consisted of a row of vertical bars, 3.8 cm in diameter, with a centerline pitch of 8.9 cm, located 48.3 cm (0.938C) upstream of the vane nose point. To help clean the wax particles from the mainstream flow, HVAC filters were installed in the closed-loop wind tunnel at a location downstream of the test section with an enlarged flow area.

The external surface of the test vane was a 3.55 times scale geometry of the vane model used by Hylton *et al.* [13], and it was approximately 7 times larger than a typical commercial airplane engine first stage vane. The test vane had a chord length of C = 51.5 cm (linear distance from stagnation point to tail point) and a span height of 54.8 cm. The pitch between stagnation lines of the vane passages was 45.7 cm. The stagnation line and pressure distribution for the test airfoil has been experimentally verified to match the design intent. The test section was designed so that the test model could be easily and precisely replaced with a geometrically identical one, which allowed for different material conductivities to be used for the model in this study.

An approximately adiabatic vane model was used to measure adiabatic film effectiveness of the film cooling. This model was constructed from polyurethane foam with a conductivity of k = 0.048 W/m·K. A higher conductivity model was used to include the conjugate heat transfer of the internal and external convective cooling and the conductive heat transfer in the wall. This model was designed so that the balance of convective and conductive heat transfer (as quantified by the Biot number) matches between the experimental model and the engine condition. As a result, the surface temperatures from this model yield overall cooling effectiveness values that match engine hardware. This "matched-Biot number" model was constructed from Corian material, manufactured by DuPont, with a conductivity of k = 1.06 W/m·K. This generated a distribution of Biot numbers that was generally representative of high pressure turbine vane designs, although it was not meant to exactly simulate a specific design. Representative Bi values for the model used in this study are given in Table 1, with Bi defined as noted in the nomenclature. The matched-Bi modeling technique is discussed in more detail by Albert and Bogard [12].

Table 1. Representative *Bi* values for the matched-*Bi* model

	PS	SS
k_{wall} (W/mK)	1.06	
t_{wall} (mm)	13	
h_f (W/m^{2}K) [12]	40	70
Bi	0.5	0.9

A secondary flow loop powered by a 7.5 hp blower provided cooling air to the vane model. The secondary flow was drawn from the tunnel mainstream by the blower, and then it passed it through a heat exchanger cooled by liquid nitrogen before splitting into the two dedicated cooling air circuits for the vane model. The vane cooling channels are shown in Fig. 2 – the "U-bend" coolant passage flowed up the forward internal channel, turned 180°, and flowed down the middle channel. The "radial" coolant passage flowed straight up the aft channel. Cooling air flow rates were controlled inlet and outlet valves, and orifice flow meters were used to measure the flow rates.

Note in Fig. 2 that the trailing edge of this airfoil model is uncooled. This is not indicative of typical turbine airfoil designs. The models in this facility were constructed with an uncooled trailing edge because the regions of interest in this and related studies were away from the trailing edge. Incorporating a cooled trailing edge would add considerably complexity to the facility design, construction, and operation, so an uncooled trailing edge was deemed to be an acceptable simplification for this experimental model.

Both versions of the vane model (low conductivity and matched-Bi) incorporated removable hatches on the pressure and suction sides, as shown in Fig. 2, that allow for relatively quick changes in cooling hole configuration. For the current study, only the forward pressure side hatch was changed when switching between standard and trenched cooling holes. The other three hatches did not have any film cooling holes, and they remained unchanged for all experiments. The hatches were constructed of the same material as the vane model in which they were installed, and they were secured with small threaded connectors located outside the region of interest for measurements. The perimeters of the low conductivity polyurethane foam hatches were sealed with foam weather stripping and vacuum grease. The perimeters of the matched-Bi Corian hatches were sealed with a non-hardening heat transfer compound. The thermal discontinuities of the hatch perimeters had a small effect on the surrounding temperatures, which was negligible for the purposes of the current study.

Table 2. Summary of experimental parameters

Vane chord length, C = 51.5 cm	Cooling hole dia., d = 4.22 mm
Vane span height = 54.8 cm	***Showerhead:*** surface angle, α = 25°, compound angle, β = 90°, spanwise pitch, p = 5.6d, length = 7.3d
Mainstream velocity, U_∞ = 5.8 m/s	
Turbulence intensity, Tu = 20%	***PS film:*** surface angle, α = 30°, compound angle, β = 0°, spanwise pitch, p = 3.0d, length = 6.2d (without trench)
Turbulence integral length scale, Λ = 3.7 cm	
Mainstream exit Re_C = 7.0x10^5	Coolant channels Re_{Dh} = 2.0x10^4
Mainstream temp., T_∞ = 305 K	Coolant temp., T_c = 220 K Density ratio, DR= 1.4

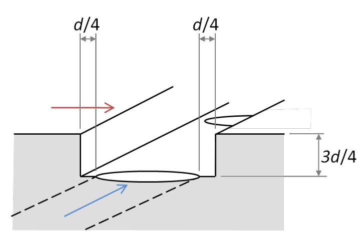

Figure 3. PS film row trenched cooling hole schematic

All film cooling holes in the vane models had a diameter of d = 4.22 mm. The vane model incorporated a three-row showerhead design, with one row biased towards the pressure side ($s = 1.65d$) and two rows biased towards the suction side ($s = 1.65d$ and $4.95d$). The showerhead consisted of straight, cylindrical holes, all of which have a surface angle of $\alpha = 25°$, a compound angle of $\beta = 90°$ with respect to the streamwise direction, and a centerline-to-centerline pitch of $p = 5.6d$ in the spanwise direction. Each row was staggered a half-pitch in the spanwise direction from the adjacent row. A row of pressure side body film cooling holes was located at $s = 32d$ from the stagnation line.

The "standard" design of body film holes consisted of straight, cylindrical holes that had a surface angle of $\alpha = 30°$, a compound angle of $\beta = 0°$, and a centerline-to-centerline pitch of $p = 3d$ in the spanwise direction. The "trenched" design of body film holes was the same as the standard design except the hole exits were situated in a spanwise, recessed trench of rectangular cross-section, with dimensions as shown in Fig. 3. The trenched hole break-out location at the floor of the trench was exactly beneath the standard hole breakout location on the airfoil surface.

Experiments were performed using a mainstream temperature of T_∞ = 305 K and a coolant temperature of about T_c = 220 K to establish a coolant-to-mainstream density ratio of DR = 1.4, unless otherwise noted. For all experiments, the mainstream approach velocity was $U_{\infty,\mathrm{approach}}$ = 5.8 m/s, as measured by a Pitot-static probe, which corresponded with an exit velocity of 22 m/s at the vane trailing edge. The Reynolds number was $Re_{C,exit} = 7.0\times10^5$, when calculated using the airfoil chord length C and the exit velocity. The mainstream turbulence characteristics were measured across a plane 14.5 cm (0.282C) upstream of the vane nose point, or 33.8 cm (0.656C) downstream of the grid bars centerline. This yielded a turbulence intensity of Tu = 20% and an integral length scale of Λ = 3.7 cm (Λ/C = 0.072). These turbulence characteristics did not include the effects of the wax sprayer, which is described later. Since the sprayer was embedded in one of the turbulence generation rods, and the turbulence rods generated very high turbulence levels, the sprayer was not expected to significantly alter turbulence levels.

The coolant flow rates through the U-bend and radial channels were set to establish Reynolds numbers based on hydraulic diameters of nominally Re_{Dh} = 20,000 for all blowing ratios. The total film cooling flow rate was determined by taking the difference between the measured inlet and exit coolant flow rates through the U-bend channel. The film cooling flow splits between the showerhead rows and the pressure side row were determined analytically using the airfoil external pressure distribution, the common supply pressure for all cooling holes, and the measured discharge coefficients of the cooling holes. The showerhead blowing ratio, M^*_{Shd}, was calculated considering all three rows combined, and it was a function of the mainstream approach velocity. The pressure side blowing ratio, M_{PS}, was calculated as a function of the local mainstream velocity at the hole exits.

The external surface temperatures of the model were measured using infrared cameras, and these data were used to determine adiabatic film effectiveness (η) and overall cooling effectiveness (ϕ). The IR cameras viewed the model through salt crystal windows in the test section wall and ceiling. They were calibrated *in situ* using thermocouples mounted on the model surface as described by Albert and Bogard [12].

All uncertainties were calculated using the sequential perturbation method [14], and they are summarized here along with the most significant sources of uncertainty. The precision uncertainty for overall cooling effectiveness was $\delta\phi = \pm0.015$. Adiabatic effectiveness had a higher uncertainty of $\delta\eta = \pm0.022$ due to corrections for conduction errors in the approximately adiabatic model. The conduction correction is summarized by Albert and Bogard [12]. These uncertainties applied equally to both the local and laterally-averaged effectiveness measurements, and they were dominated by the IR camera calibration uncertainty of $\delta T_{wall,ext} = \delta T_{aw} = \pm1.3$ K. Uncertainties for the blowing ratios were dominated by the measurements of the orifice meter pressure differentials, $\delta(\Delta P_{inlet}) = \delta(\Delta P_{outlet}) = \pm2.5$ Pa, and the film cooling hole discharge coefficients, $\delta(C_d) = \pm0.1$ (low M) to ±0.01 (high M). The uncertainty in the blowing ratios was $\delta M^*_{Shd} = \delta M_{PS} = \pm0.25$, which applied equally across low and high blowing ratios. The uncertainties of the mainstream flow conditions were $\delta Tu = \pm1.2\%$ (i.e., ±6% of the measured turbulence intensity of Tu = 19.9%), $\delta\Lambda = \pm0.8$ cm, $\delta U_{\infty,approach} = \pm0.08$ m/s, and $\delta Re_{C,exit} = \pm9{,}000$. All uncertainties were consistent with numerous repeatability checks of data recorded at the same conditions in different experiments.

A device to spray molten wax droplets into the wind tunnel mainstream flow was designed and constructed for this study. Figure 4 shows a schematic of this device and a photograph of the sprayer situated in the mainstream turbulence grid. The wax spray device was built around a commercially available, pneumatically-actuated, air atomizing spray nozzle (Spray Systems Co. 63067-1/8JJAUCO). The spray nozzle was situated in a section of 1" nominal diameter PVC pipe (3.3 cm O.D.), which also housed the egress of the molten wax supply line, the heated atomizing air supply and exhaust lines, and the actuating air line. The continuous flow of the heated atomizing air served to keep the molten wax above its solidification temperature. The wax line was supplied by a molten wax reservoir that was kept warm with an electrical resistance heating wrap. The air lines were supplied by facility compressed air. The atomizing air line passed through a pressure regulator and an electrical resistance air process heater before coming in contact with the molten wax line. Just before entering the spray nozzle, the heated atomizing air line split into a sprayer supply line and an exhaust line. The exit of the exhaust line (outside of the wind tunnel) was controlled with a valve and fitted with a pressure gage to monitor the pressure of the atomizing air at the nozzle. Variable autotransformers were used to control the voltage to the air and wax heaters. The sprayer/PVC pipe assembly entered the wind tunnel test section through a hole in the test section ceiling. When installed the sprayer/PVC pipe assembly took the place of one of the turbulence grid bars.

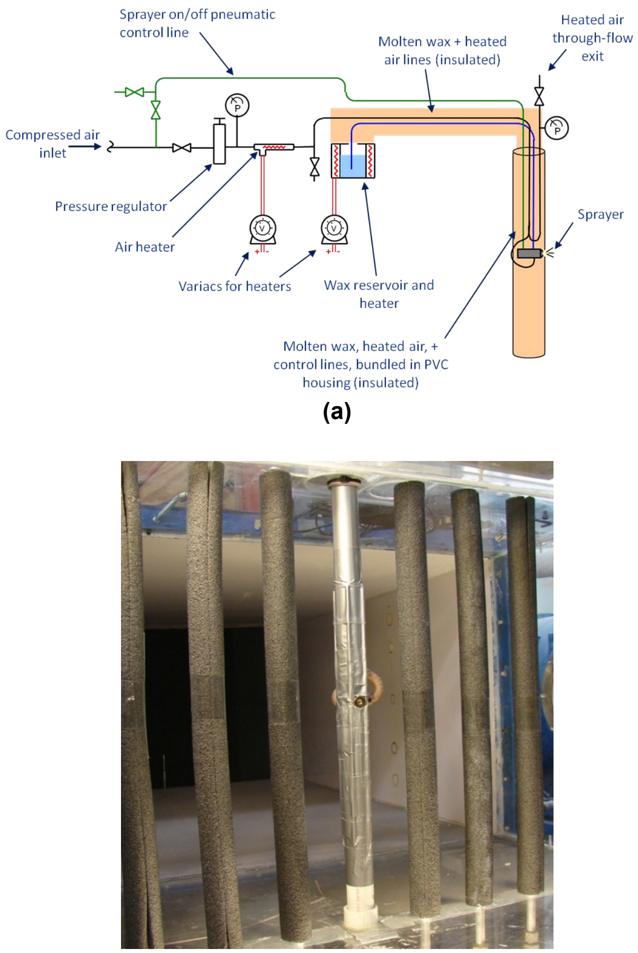

(a)

(b)

Figure 4. Wax spray device (a) schematic and (b) photo *in situ*

The wax used for these experiments was purchased from Rubitherm Technologies GmbH (Berlin, Germany), and it had a nominal solidification temperature of $T_{wax,solid}$ = 42°C = 315 K. This specialty wax was selected based on a preliminary analysis of the convective time and length it takes for molten wax droplets to solidify in the wind tunnel mainstream flow. It was desirable for the wax droplets to be at least partially molten when impacting the model surface, in order to best simulate the physics of the deposition process that occurs for coal ash particles in an actual turbine flowpath. Details of this analysis were provided by Albert *et al.* [7] for this same wax spray device applied to a similar facility.

Wax droplets of a certain size were created in the wind tunnel mainstream flow in order to match the Stokes number of coal ash particles in the actual engine flowpath. By matching the Stokes number, the wax droplets follow the flow field in the same manner as coal ash particles would in engine conditions. An analysis was performed to determine the target size for the wax droplets in the current study, which used the following formula for a spherical particle in a fluid flow, from Hinds, 1999 [15].

$$Stk = \frac{\tau}{l_{char}/U_{char}} = \frac{\rho_p d_p^2 U_{char}}{18\, l_{char} \mu_g} \tag{1}$$

The Stokes number is essentially a ratio of the time it takes for an aerosol particle to respond to changes in the fluid flow field, τ, versus the time it takes for a particle to travel past a flow obstacle of some characteristic length, l_{char}/U_{char}. Particles with $Stk \ll 1$ will follow the flow very closely and therefore will not cause significant amounts of inertial deposits. Particles with $Stk \geq 1$ do not follow the surrounding flow as well, so they are more likely to impact flow boundaries and cause deposits on turbine airfoils. The current study is primarily concerned with the inertial deposition of larger particles, with $Stk \geq 1$, so these larger particles are of interest when matching the Stokes numbers between engine and the wind tunnel conditions.

For this matched-Stokes number analysis, the engine coal ash particles were assumed spherical, with a density of ρ_p = 1.98 g/cm^3, based on information given in Bons *et al.* [16]. Bons *et al.* also estimated the pertinent size of coal ash particles depositing on turbine airfoils in syngas-fueled engines to be in the range 1-10 μm, based on the performance of the advanced filtration systems of these engines. No other substantiated, specific data of coal ash particle sizes in syngas-fueled gas turbines have been found in the public literature by the current authors, so the 1-10 μm estimate by Bons *et al.* is used in the current study. An engine scale cooling hole diameter of d = 0.32 mm was used as the characteristic length scale in Eqn. (1) to yield a Stokes number range of Stk_d = 1-100 for a coal ash particle size range of d_p = 1-10 μm in engine conditions. To match these Stokes numbers in the wind tunnel conditions, the desired wax droplet size is nominally 8X larger than the engine particles, $d_{p,wax}$ = 8-80 μm.

In order to assess the wax particle sizes created in the current experimental facility, samples of the wax spray were captured in the tunnel facility at typical test conditions using small coupons. These coupons were viewed using a scanning electron microscope (SEM), and a representative image is included as Fig. 5. This showed that the wax droplets have a wide range of sizes that include the desired size of approximately 8-80 μm. The distribution of particle sizes was not quantified because it was viewed as of minor importance relative to the sizes of the largest particles when modeling inertial deposition. The region of interest for the current study is the leading edge and pressure side of an airfoil. The vast majority of the deposit thickness on these surfaces come from the largest particles in the aerosol flow because they have by far the largest mass and inertia.

Figure 5 suggests that the wax particles generated in this study were somewhat irregularly shaped, not spherical as was modeled by Eqn. 1. This discrepancy is not significant because the movement of a small particle is dominated by its inertia and aerodynamic drag, which are insensitive to exact particle shape. Considering the irregularly shaped bodies in Fig. 5 as spheres yields a reasonable estimate of their inertial mass. Aerodynamic drag at low (relative) Reynolds numbers is a weak function of body shape.

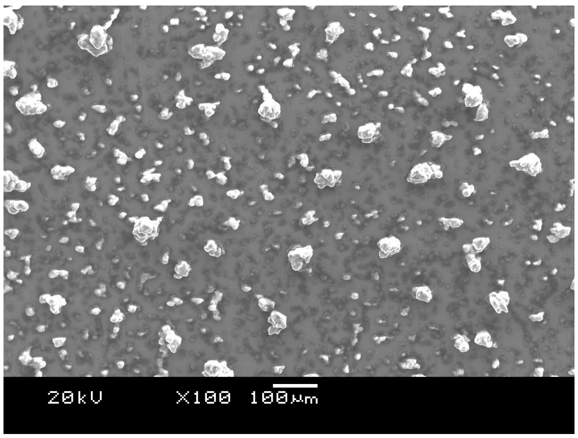

Figure 5. Scanning electron microscope image of wax spray sample

For a typical deposition experiment, the wind tunnel facility was brought to the desired flow conditions (see Table 2) and held at steady state for at least 15 minutes, which was more than enough time to ensure the model temperatures were steady. The wax spray was started and maintained for 30 minutes for all test cases. Wind tunnel operating conditions were held very constant during the wax spray, and instrumentation data was recorded every 30-60 seconds to verify this after the experiment. The average wax mass flow rate during an experiment was approximately 4 g/min, as determined by weighing the wax reservoir before and after each experiment. Most of the sprayed wax passed through the test section without depositing on the model. The target area of the wax spray jet was roughly the middle half of the airfoil span, and the jet center was biased slightly to the pressure side of the stagnation line. A substantial portion of the wax spray passed to the suction side of the stagnation line, but very little of it deposited on the mid-chord and aft portion of the airfoil suction side. After each experiment the vane was photographed and deposit thicknesses were measured at certain locations using a pin depth gauge. The deposit thicknesses measurements were typically repeatable within $\delta t_{dep} = \pm 0.2$ mm $= \pm 0.05d$.

RESULTS

This section presents photographs from different experiments that show the range of deposit features created on the models and some of their interesting details. In these photographs, the stagnation line is shown schematically with a dashed red line. The pressure surface of the vane extends to the left of the stagnation line, with the trailing edge typically visible at the left of each photo. The forward portion of the suction surface is visible at the right of each photo. The portion of the suction side not visible in the photos always had very thin and sparse deposits.

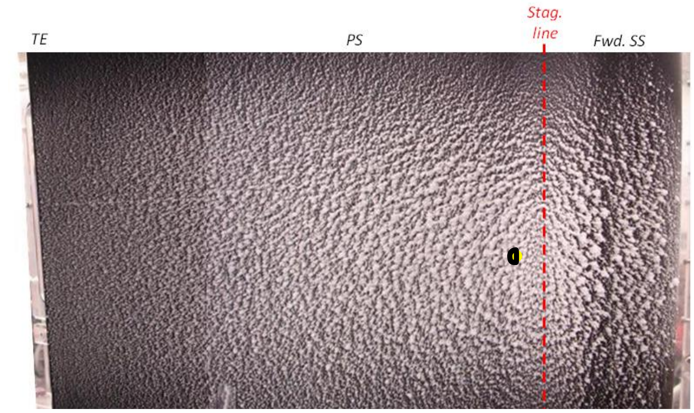

Figure 6. Photo of deposits: Non-film-cooled, isothermal vane ($T_\infty = T_c = 305$ K)
[maximum $t_{dep} = 3.1$ mm at location marked by a circle]

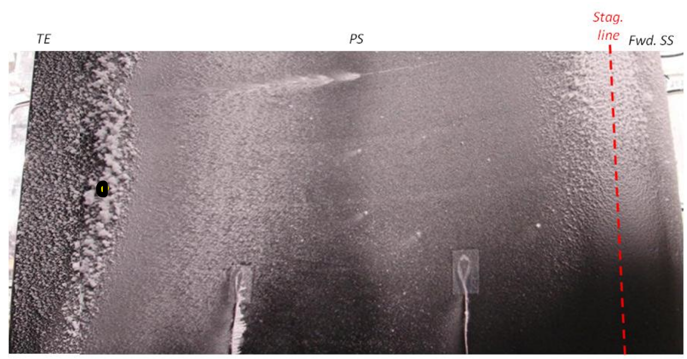

Figure 7. Photo of deposits: Non-film-cooled, internally cooled vane ($T_\infty = 305$ K, $T_c = 220$ K, $DR = 1.4$)
[maximum $t_{dep} = 5.3$ mm at location marked by a circle]

It is important to note that all deposits shown in these photographs reached an equilibrium condition, at which the deposit thickness no longer changed. This was likely caused by a balance between the amount of wax particles deposited on the surface and the amount of particles liberated from the surface by fluid or impaction forces. The erosion of deposited particles was visibly evident after the first several minutes of wax spray. This equilibrium condition typically developed after about 10 to 15 minutes of wax spray, and the wax spray lasted 30 minutes for all cases. This approach to an equilibrium deposit thickness was also observed by Albert *et al.* [7] using the same wax spray technique with a turbine blade leading edge model; they presented measurements of model surface temperature and deposit thickness variation with time to further substantiate this observation. As noted in the Introduction section, some other researchers have found that deposit thickness approaches an equilibrium condition, while other do not mention it. It is not clear to what extent this equilibrium condition occurs for ash deposits on gas turbine surfaces.

Initial experiments with the wax spray technique in the current study were performed using a non-film-cooled vane model constructed of a conducting material such that the model matches the Biot number of a turbine airfoil at engine conditions. Figure 6 presents a photograph of the deposits formed on this non-film-cooled model when the internal coolant temperature was equal to the mainstream temperature, which resulted in an isothermal vane with no symptoms of the internal cooling scheme present on the airfoil external surface. The deposits shown in Fig. 6 had an intricate texture, but there were no sudden changes in the maximum deposit thicknesses along the airfoil surface. The deposits are thickest adjacent to the stagnation line (maximum t_{dep} = 3.1 mm), and they become gradually thinner towards the trailing edge.

In another experiment, the same non-film-cooled, matched-*Bi* vane model was used when the internal coolant temperature was cooled to T_c = 220 K, which is consistent with a coolant-to-mainstream density ratio of *DR* = 1.4. The resulting deposits are shown in Fig. 7, which illustrates that the deposition was clearly influenced by changes in vane surface temperature, even with no film cooling flows present. There were moderately thick deposits in the leading edge region of the airfoil that transition to very thin, yet visible, deposits over most of the pressure surface.

The thickest deposits on the cooled airfoil were towards the trailing edge of the airfoil, as shown in Fig. 7, with a maximum thickness of t_{dep} = 5.3 mm. These thick deposits in the trailing edge region were attributed to the lack of internal cooling in this region, which caused higher local surface temperatures and a resulting increase in deposit thickness. As shown in Fig. 2 and discussed previously, the trailing edge for this experimental model was left uncooled for simplicity because the region of interest in this and related studies is away from the trailing edge. A fortuitous result of this simplification is that the uncooled trailing edge provided a dramatic demonstration of the sensitivity of deposit formation to surface temperature. The thick deposits on the uncooled trailing edge region were evident in all test cases using the cooled, matched-*Bi* model, regardless of film cooling configuration.

It was observed in numerous experiments that higher surface temperatures led to increased deposit thickness. The photos in Figs. 6 and 7 are a clear illustration of this. Furthermore, there was evidence from the current study, discussed later, that shows evidence of a threshold surface temperature above which deposits grow substantially thicker.

Figure 8 shows the deposits formed on the film-cooled version of the matched-*Bi* model with active showerhead and standard PS film cooling holes. For this condition, the blowing ratio of all cooling holes was $M_{PS} = M^*_{Shd} = 2.0$. These deposits were moderately thick in the showerhead region, very thin over most of the pressure surface, and suddenly became much thicker at the uncooled trailing edge as discussed previously. There were small regions of more dense deposits just downstream of the PS film cooling holes, which formed in the recirculation regions underneath the coolant jets detaching from the surface. In the showerhead region the deposits are also clearly influenced by the coolant jets (see also Fig. 10a).

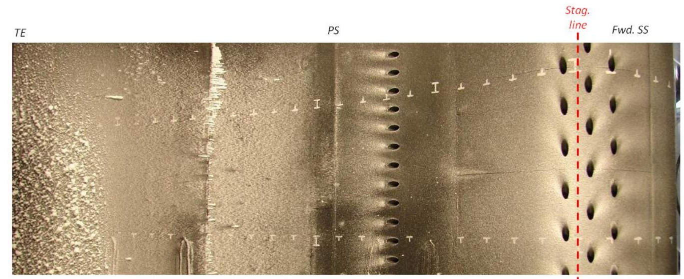

Figure 8. Photo of deposits: Film-cooled, matched-*Bi* vane with standard PS holes (M_{PS} = 2.0, M^*_{Shd} = 2.0, *DR* = 1.4)

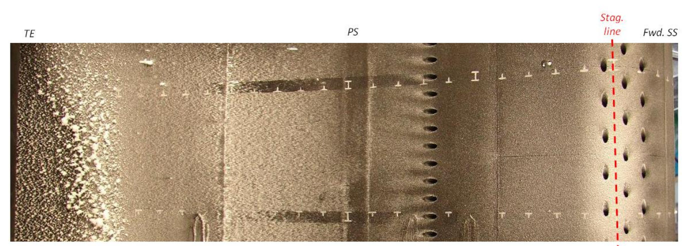

Figure 9. Photo of deposits: Film-cooled, matched-*Bi* vane, with standard PS holes, lower blowing ratio (M_{PS} = 1.0, M^*_{Shd} = 0.75, *DR* = 1.4)

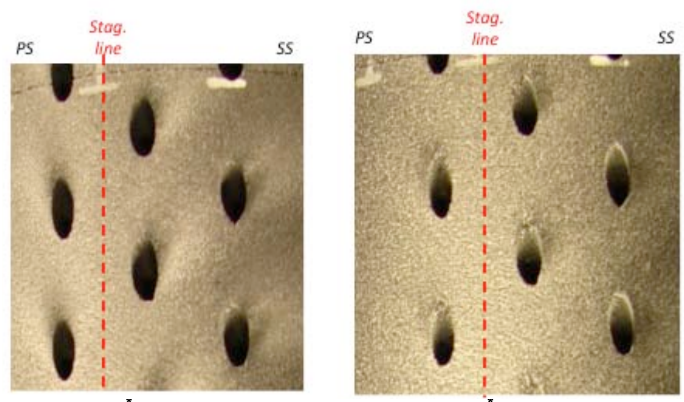

(a) M^*_{shd} = 2.0 **(b) M^*_{shd} = 0.8**

Figure 10. Detailed photos of deposits at showerhead for different blowing ratios (*DR* = 1.4)

The deposits formed on the vane operating at a lower blowing ratio are shown in Fig. 9. Away from the cooling holes there were few differences between the higher and lower blowing ratios. Near the PS film cooling holes, the M_{PS} = 1.0 (Fig. 9) case did not have the small regions of denser deposits just downstream of the holes, which was different from the M_{PS} = 2.0 (Fig. 8). This was because the coolant jets remained attached to the surface at the lower blowing ratio. The showerhead holes for the lower blowing ratio case had deposits that formed inside the cooling hole exits. This occurred because the coolant jets were swept downstream before they could fully fill the showerhead hole exits. Detailed views of the showerhead regions in Figs. 8 and 9 are shown in Fig. 10.

To further study the effect of surface temperature on deposit formation, a low conductivity ("adiabatic") version of the film cooled vane model was used in a wax spray experiment, with the resulting deposits shown in Fig. 11. For this case, the flow conditions and temperatures were the same as for the matched-*Bi* model case shown in Fig. 8 but the surface temperatures were significantly warmer. Much thicker deposits formed on the pressure surface of the adiabatic model than the conducting model. Again, this was attributed to the warmer surface causing more deposit accumulations. A detailed comparison of the pressure side holes for the matched-*Bi* model and the adiabatic model is shown in Fig. 12. As seen in Fig. 12b, the thicker deposits on the adiabatic model ended where the PS film holes exit. There were thin ridges of deposit extended just past the cooling holes of the adiabatic model.

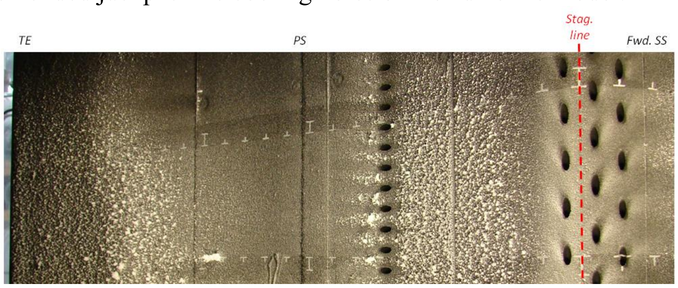

Figure 11. Photo of deposits: Film-cooled, low-conductivity vane with standard PS holes (M_{PS} = 2.0, M^*_{Shd} = 2.0, DR = 1.4)

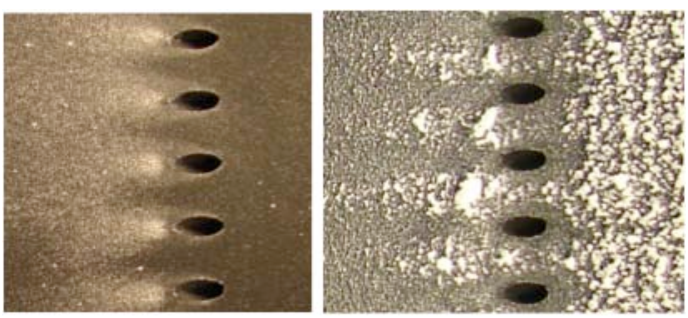

(a) Matched-Bi model **(b) Adiabatic model**

Figure 12. Detailed photos of deposits at standard PS film holes for different model conductivities (DR = 1.4)

Vane surface temperature measurements suggest there was a threshold surface temperature above which deposits grew significantly thicker. Consider the condition of the vane with showerhead and standard PS holes operating at a blowing ratio of $M^*_{Shd} = M_{PS} = 2.0$. Measurements of laterally-averaged overall cooling effectiveness (ϕ) and adiabatic film effectiveness (η) for this condition are shown in Fig. 13. (Albert and Bogard [12] discuss these η and ϕ measurements in more detail.) Figure 14 presents measurements of laterally-averaged deposit thickness from both the matched-*Bi* model (used to measure ϕ) and the low-conductivity model (used to measure η). The data in Fig. 14 were from measurements of the deposits shown in Figs. 8 and 11. Note that the only region of thicker deposit on the matched-*Bi* model occurred for s/d > 95, which corresponds to the uncooled trailing edge as previously discussed. The regions of thicker deposits on the low-conductivity model were s/d = 5 to 40 and s/d > 65. As shown in Fig. 13, these regions of thicker deposits for both models corresponded to surface temperatures above approximately $\eta = \phi = 0.12$, which corresponded to T_{surf} = 295 K.

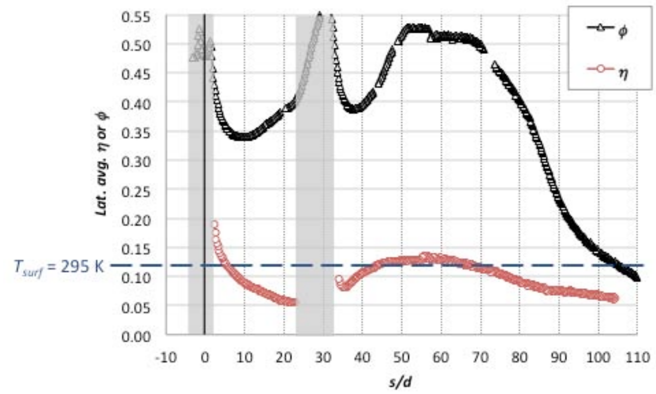

Figure 13. Laterally averaged η and ϕ for the vane with showerhead + standard PS holes, prior to deposition (M_{PS} = 2.0, M^*_{Shd} = 2.0, DR = 1.4)
These data correspond to the conditions used to simulate deposits shown in Figs. 8 and 11.

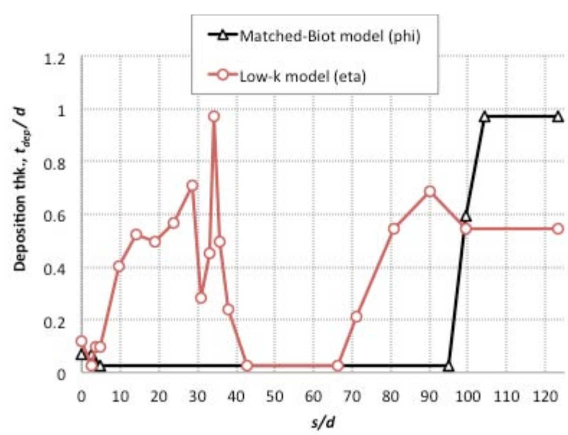

Figure 14. Laterally averaged deposit thickness for the vane models with showerhead + standard PS holes (M_{PS} = 2.0, M^*_{Shd} = 2.0, DR = 1.4)
These data correspond to the deposits shown in Figs. 8 and 11.

These data suggest that there was a threshold surface temperature of 295 K for these wax spray deposition experiments above which deposits grew substantially thicker. This is primarily a function of surface temperature because the mainstream and film coolant flow fields are nearly identical between the two cases considered in Figs. 13 and 14. A threshold gas temperature for increased deposit thickness has been reported for engine condition deposition experiments by other researchers (e.g., Wenglarz and Fox [3], Crosby *et al.*

[4]). This is an important similarity between the experimental technique of the current study and the engine condition deposition process it is modeling.

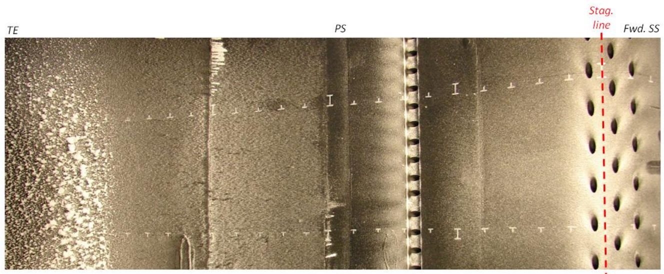

Figure 15. Photo of deposits: Film-cooled, matched-*Bi* vane with trenched PS holes, (M_{PS} = 2.0, M^*_{Shd} = 2.0, DR = 1.4)

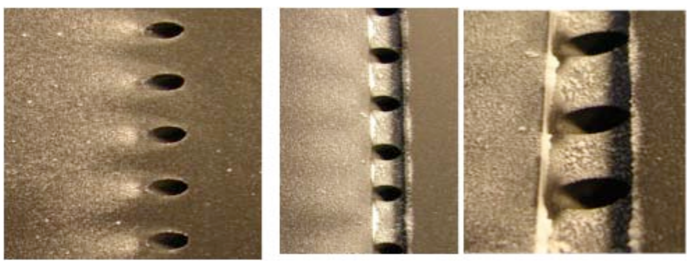

(a) Baseline PS holes **(b) Trenched PS holes**

Figure 16. Detailed photos of deposits at standard and trenched PS film holes (DR = 1.4)

The deposit that formed near the trenched film cooling holes is shown in Figs. 15 and 16b. These photos show that deposits accumulated in the trench to a greater extent than the standard PS holes at the same blowing ratio (Figs. 8 and 12a). The thickest deposits in the trench were at the downstream wall between cooling hole exits with a typical thickness of t_{dep}/d = 0.4. The bottom surface and the upstream wall of the trench had thin deposits that were within the uncertainty of the thickness measurement, t_{dep}/d < 0.05. The thinnest deposits in the trench were at the coolant jet impingement locations on the downstream wall. Also note that the deposits on the upstream edge of the trench were thinner very near the cooling holes, which was likely due to the lower local surface temperatures caused by convective cooling in the holes. The deposits that formed downstream of both PS hole configurations were very thin, but were more uniform for the trenched holes, as shown in Fig. 16. Elsewhere on the pressure surface, the deposits were very similar between the trenched holes case (Fig. 15) and the standard holes case (Fig. 8). One of the cooling holes in the trenched model was inadvertently shifted in the spanwise direction (Fig. 16b), but this did not have a significant effect on these results.

Measurements of adiabatic film effectiveness were performed on the vane pressure side before and after deposit formation, for both the baseline and trenched hole configurations. (For the post-deposition measurements, the deposits were painted flat black to allow for accurate infrared camera measurements.) Comparisons of laterally-averaged adiabatic film effectiveness measurements for these cases are shown in Fig. 17. These data show very little difference in the laterally-averaged film performance for either film configuration, even though this adiabatic model did have significant deposit thicknesses downstream of the showerhead holes (see Fig. 11). The insensitivity of the film performance to the surface roughness generated by the deposits may be attributable to the strong disturbance the showerhead cooling had on the pressure side flow. The showerhead cooling jets helped to establish higher turbulence along the pressure side boundary layer so that the film cooling was less sensitive to the relatively small surface roughness caused by the deposits.

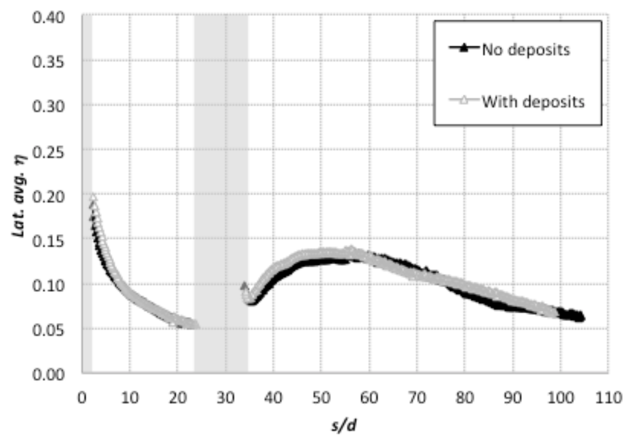

(a) Baseline PS holes

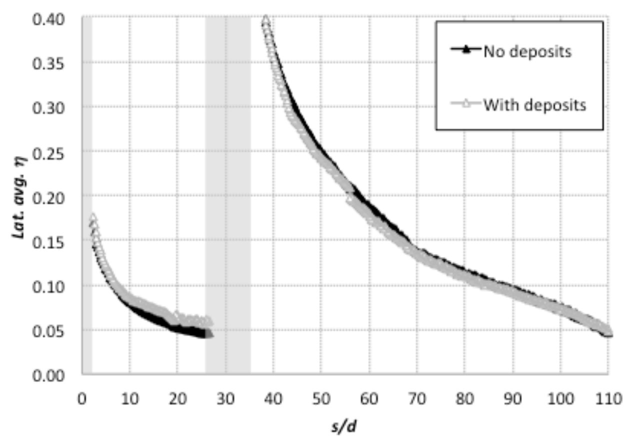

(b) Trenched PS holes

Figure 17. Effect of deposits on laterally-averaged η for standard and trenched PS film holes (M_{PS} = 2.0, M^*_{Shd} = 2.0, DR = 1.4)

To illustrate this film performance comparison further, contour plots of adiabatic film effectiveness are presented in Fig. 18, which correspond to the data in Fig. 17 for the baseline hole configuration before and after deposition. As can be seen in the contour plots, the deposits do affect local values of adiabatic film effectiveness, particularly where the deposits are thickest just upstream of the PS holes. However, these effects become very small in terms of the laterally averaged data.

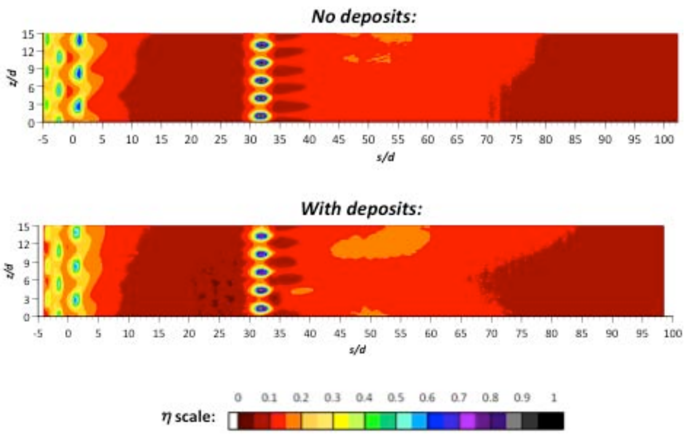

Figure 18. Effect of deposits on η contours for standard and trenched PS film holes (M_{PS} = 2.0, M^*_{Shd} = 2.0, DR = 1.4)

CONCLUSIONS

For this study a new experimental technique for modeling contaminant deposition on turbine component surfaces was utilized to study the pressure side of a turbine vane airfoil. The focus of this study was the leading edge and pressure side of the vane. Experiments were conducted on two vane models with different thermal conductivities, which isolated the effects of surface temperature on deposit formation. Two pressure side film cooling configurations were studied: a standard hole design and an advanced trenched hole design.

The deposits created in this study reached an equilibrium thickness after about 10 to 15 minutes. All final results were obtained using 30 minutes of deposition time, so these deposits were essentially steady state results.

The surface temperature of the vane model had a substantial influence on the deposit formation. This was observed when testing a non-film-cooled vane model with different internal cooling conditions. This was also observed with the film cooled models made of different thermal conductivities and operating at the same cooling flow conditions. Furthermore, the local increase in surface temperature in the matched-Biot number model caused by the uncooled trailing edge resulted in a sharp increase in deposit thickness. (The uncooled trailing edge was a simplification used for this model that is not representative to typical engine hardware.) A threshold surface temperature was evident in the experiments, above which the deposits grew substantially thicker.

Film cooling blowing ratio had a noticeable but minor influence on deposit formation. The deposits revealed symptoms of the different flow fields for the blowing ratios tested, such as coolant jet detachment from the surface.

Experiments using the trench configuration for film cooling holes showed that deposits would accumulate within the trench, particularly on the downstream wall between hole exits. However, this buildup was relatively small and did not appear to significantly change the film cooling flow in the trench.

Measurements of adiabatic film effectiveness were performed before and after deposits formed for both standard and trenched pressure side film cooling holes. These measurements showed no appreciable degradation of film cooling performance for either configuration due to the presence of the deposits. This was likely because the showerhead cooling jets generated higher turbulence along the pressure side, which made the boundary layer less sensitive to the surface roughness of the deposits.

ACKNOWLEDGMENTS

This work was primarily supported by U. S. Department of Energy, National Energy Technology Laboratory (NETL) through the University Turbine Systems Research (UTSR) program, which has been coordinated by the South Carolina Institute for Energy Studies (SCIES) at Clemson University. Additional support was provided by the U. S. Department of Defense, Office of Naval Research (ONR) through the Electric Ship Research and Development Consortium (ESRDC).

The views expressed in this publication are those of the authors and do not reflect the official policy or position of the U. S. Government.

REFERENCES

[1] Walsh, P. M., Sayre, A. N., Loehden, D. O., Monroe, L. S., Beér, J. M., and Sarofim, A. F., 1990, "Deposition of Bituminous Coal Ash on an Isolated Heat Exchanger Tube: Effects of Coal Properties on Deposit Growth," *Progress in Energy and Combustion Science*, Vol. 16, pp. 327-346.

[2] Rosner, D. E., and Nagarajan, R., 1987, "Toward a Mechanistic Theory of Net Deposit Growth from Ash-Laden Flowing Combustion Gases: Self-Regulated Sticking of Impacting Particles and Deposit Erosion in the Presence of Vapor Deposited – or Submicron Mist – 'Glue,'" AIChE Symposium Series, Heat Transfer – Pittsburgh 1987, pp. 289-296.

[3] Wenglarz, R. A. and Fox, R. G., 1990, "Physical Aspects of Deposition From Coal-Water Fuels Under Gas Turbine Conditions," *Journal of Engineering for Gas Turbines and Power*, Vol. 112, pp. 9-14.

[4] Crosby, J.M., Lewis, S., Bons, J.P., Ai, W., and Fletcher, T.H., 2008, "Effects of Temperature and Particle Size on Deposition in Land Based Turbines," *Journal of Engineering for Gas Turbines and Power*, Vol. 130.

[5] Ai, W., Laylock, R.G., Rappleye, D.S., Fletcher, T.H., and Bons, J.P., 2009, "Effect of Particle Size and Trench

Configuration on Deposition from Fine Coal Flyash Near Film Cooling Holes," ASME Paper No. GT2009-59571.

[6] Lewis, S., Barker, B., Bons, J.P., Ai, W., and Fletcher, T.H., 2011, "Film Cooling Effectiveness and Heat Transfer Near Deposit-Laden Film Holes," *Journal of Turbomachinery*, Vol. 133.

[7] Albert, J.E., Keefe, K.J., and Bogard, D.G., 2009, "Experimental Simulation of Contaminant Deposition on a Film Cooled Turbine Airfoil Leading Edge," ASME Paper No. IMECE2009-11582.

[8] Lawson, S.A., and Thole, K.A., 2010, "Simulations of Multi-phase Particle Deposition on Endwall Film-Cooling," ASME Paper No. GT2010-22376.

[9] Bunker, R.S., 2002, "Film Cooling Effectiveness Due to Discrete Holes Within a Transverse Surface Slot," ASME Paper No. GT2002-30178.

[10] Waye, S.K., and Bogard, D.G., 2007, "High-resolution Film Cooling Effectiveness Measurements of Axial Holes Embedded in a Transverse Trench with Various Trench Configurations," *Journal of Turbomachinery*, Vol. 129, No. 2, pp. 294-302.

[11] Dorrington, J.R., Bogard, D.G., and Bunker, R.S., 2007, "Film Effectiveness Performance for Coolant Holes Embedded in Various Shallow Trench and Crater Depressions," ASME Paper No. GT2007-27992.

[12] Albert, J.E., and Bogard, D.G., 2011, "Measurements of Adiabatic Film and Overall Cooling Effectiveness on a Turbine Vane Pressure Side with a Trench," ASME Paper No. GT2011-46703.

[13] Hylton, L.D., Milhec, M.S., Turner, E.R., Nealy, D.A., and York, R.E., 1983, "Analytical and Experimental Evaluation of the Heat Transfer Distribution Over the Surface of Turbine Vanes," NASA CR 168015.

[14] Moffat, R.J., 1988, "Describing the Uncertainties in Experimental Results," *Experimental Thermal and Fluid Science*, Vol. 1, pp. 3-17.

[15] Hinds, W. C., 1999, Aerosol Technology: Properties, Behavior, and Measurement of Airborne Particles, 2nd edition, Wiley-Interscience, New York, NY.

[16] Bons, J. P., Crosby, J., Wammack, J. E., Bentley, B. I., and Fletcher, T. H., 2007, "High Pressure Turbine Deposition in Land-Based Gas Turbines from Various Synfuels," *Journal of Engineering for Gas Turbines and Power*, Vol. 129, pp. 135-143.